AntiPD-L1 antibody conjugated Au-SPIOs nanoparticles for enhancing radiosensitivity and activating anti-tumor immune response

Chengrun Du
Fudan University Shanghai Cancer Center
Jianyun Jiang
Fudan University Shanghai Cancer Center
Caifeng Wan
Shanghai Jiaotong University
Guangsen Pan
Fudan University Shanghai Cancer Center
Fangfang Kong
Fudan University Shanghai Cancer Center
Ruiping Zhai
Fudan University Shanghai Cancer Center
Chaosu Hu
Fudan University Shanghai Cancer Center
Hongmei Ying (yinghongmei2011@sina.com)
Fudan University Shanghai Cancer Center

Research Article

Keywords: enhancing radiosensitization, high Z-material, PD-L1, TAMs polarization, immunotherapy, Au, SPIOs

Posted Date: April 22nd, 2022

DOI: https://doi.org/10.21203/rs.3.rs-1566279/v1

Abstract

To improve the radiation therapy outcomes by inducing more toxicity for tumors and less for normal tissue and switch microenvironment immunosuppressive caused by expression of PD-L1 and tumor-associated macrophages (TAMs) to immunoreactive, we designed a PD-L1-targeted nanoplatform consisting of gold nanoparticles (AuNPs) and superparamagnetic iron oxide nanoparticles (SPIOs)(antiPD-L1-SPIOs@PLGA@Au). AntiPD-L1-SPIOs@PLGA@Au targeted on the B16F10 cell membrane and in cytoplasm, and the association could be reduced by the antibody blocking. In vivo T2-weight image, the best enhancement effect of tumor was achieved two hours after intravenous injection of antiPD-L1-SPIOs@PLGA@Au. Compared with radiation alone, the Do sensitization ratios of antiPD-L1-SPIOs@PLGA@Au was 1.34. The inhibition effect of irradiation combined with antiPD-L1-SPIOs@PLGA@Au was higher than that of radiotherapy alone in the B16F10 subcutaneous tumor model. During the entire observation period, all mice in the antiPD-L1-SPIOs@PLGA@Au group lived longer than 3 weeks. AntiPD-L1-SPIOs@PLGA@Au enhancing radiosensitivity was achieved by increasing ROS production and attenuating DNA damage repair. In vitro and in vivo experiments showed that antiPD-L1-SPIOs@PLGA@Au could promote the polarization of tumor-associated macrophages (TAMs) to M1 and reverse the immunosuppressive regulation induced by TAMs. antiPD-L1-SPIOs@PLGA@Au could increase the expression of CRT in tumor, block the PD-L1/PD pathway, activate CD8+T cells, promote the increase of IFN-γ, TNF-α and IL-12 release, and finally activate the anti-tumor immune response. In conclusion, antiPD-L1-SPIOs@PLGA@Au was proved to have the ability to form targeted imaging and enhance radiosensitivity, block the PD-L1/PD-1 immune checkpoint pathway, reverse the immunosuppressive regulation caused by TAMs, successfully realizing the synergistic effect of radiotherapy combined with immunotherapy.

Introduction

Radiotherapy, alongside surgery and chemotherapy, is a mainstream cancer treatment strategy that has been extensively used in clinic to treat 65–75% of local solid tumors with curative or palliative intent [1]. The goal of radiotherapy is to maximize the radiation dose to the tumor volume while limiting off-target side effects. With the application of IMRT and SBRT which have considerable advantage in distribution of radiation dose compared with the traditional 2-dimentional radiotherapy, radiotherapy has brought significant benefit for cancer patients. However, certain cancer patients still faced treatment failure after radiotherapy, especially those patients with malignant tumor possessing the nature of radiation resistance. With the advantage of greater absorption and deposition of energy in surrounding tissues, gold nanoparticles (AuNPs) have been most extensively studied as radiosensitizer [2, 3]. Superparamagnetic iron oxide nanoparticles (SPIOs) are capable of generating T_2-weighted contrast enhancement in magnetic resonance imaging (MRI). A nanoplatform consisting of AuNPs and SPIOs can augment cancer treatment by facilitating imaging and increasing the efficacy of therapy, ultimately possessing radiotheranostic properties [4]. Moreover, SPIO recently was found to be able to polarize

tumor-associated macrophages (TAMs) from a protumor M2-like to an antitumor M1-like, switching immunosuppressive microenvironment which is crucial to the effect of radiotherapy[5].

Programmed death-ligand 1(PD-L1), a type I transmembrane protein, is expressed in the cytoplasm and the cell surface of tumor [6, 7]. Blockade of PD-1/PD-L1 axis has shown to augment T cell responses and long-term remissions in various types of tumors [8]. Radiation induces a local inflammatory response that could enhance the infiltration of tumor-specific T cells and simultaneously induce PD-L1expression in the tumor microenvironment that markedly weakens radiation-induced antitumor immunity [9]. Thus the combination of PD-L1/PD-1 axis inhibitors and RT is considered to enhance the efficacy of radiation and activating the cancer-specific immunity.

In this work, to achieve enhancing radiosensitization and triggering cancer immunotherapy simultaneously, we fabricated multifunctional poly (lactic-co-glycolic acid) (PLGA) nanoparticles using the single emulsion oil-in- water (O/W) solvent evaporation method. AuNPs were coated on the surface of PLGA, whereas SPIOs were encapsulated inside the core. The nanoparticle was conjugated with antiPD-L1 to inhibit the PD-1/PD-L1 axis and to increase the target specificity. The ability of antiPD-L1-SPIOs@PLGA@Au to target PD-L1 and radiosensitize B16F10 tumor in vitro/vivo were evaluated and the underlying mechanisms were explored.

Methods

Preparation of antiPD-L1-SPIOs@PLGA@Au

SPIOs@PLGA was prepared using single emulsion oil-in-water (O/W) solvent evaporation method [10]. Briefly, 20 mg/mL oleic-acid-coated SPIOs nanoparticles in 0.5mL hexane was mixed with 100 mg PLGA dissolved in 5mL methylene chloride. And then add the resultant organic phase dropwise to precooled aqueous solution of polyvinyl alcohol (PVA, 20 mL, 2%, w/v). After emulsification with probe sonication and evaporation by magnetic stirring, SPIOs@PLGA was obtained and dispersed in 20ml of 0.5 mol/L NaCl aqueous solution of 1mg/mL polyallylamine hydrochloride (PAH). Next, PAH-absorbed SPIOs@PLGA was mixed with 100 mL citrate-stabilized AuNPs suspension which was prepared via a redox reaction. By repeating the centrifuge/wash steps, the Au-coated SPIOs@PLGA was obtained and re-dispersed into $HAuCl_4$ solution (2 mL,1% w/v) with stirring for 30 min. Finally, SPIOs@PLGA@Au was obtained by adding hydroxylamine hydrochloride solution (NH_2OHHCl, 0.3 mL, 0.5 mol/L) and stirring the mixture to reduce HAuCl4 to form Au nanoshell.

To couple antiPD-L1 antibody with SPIOs@PLGA@Au, SH–poly (ethylene glycol) (PEG)–carboxylic acid (COOH) (SH–PEG–COOH) (5 mg) was added to SPIOs@PLGA@Au aqueous solution (1 mL, 2mg/mL) and then the free SH–PEG–COOH was removed by centrifuge/wash steps. Afterward, the precipitate was re-dispersed in phosphate-buffered saline (PBS), and the carboxylic acid groups on the surface of the pegylated SPIOs@PLGA@Au were activated by introducing 1-(3-dime-thylaminoprpyl)-3-ethylcarbodiimide hydrochloride (EDC) and N-hydroxysuccinimide (NHS) coupling activator (10 mg/10 mg). After stirring

gently at room temperature for 2 h and centrifuging/washing steps, the activated nanoparticles were mixed with anti-PD-L1 antibodies (10 mL, 77μg/mL) and incubated for 90 min in an isothermal shaker. By repeated centrifuge/wash steps, PD-L1-targeted SPIOs@PLGA@Au (antiPD-L1-SPIOs@PLGA@Au) were obtained finally.

Characterizations of antiPD-L1-SPIOs@PLGA@Au

The morphology and size of antiPD-L1-SPIOs@PLGA@Au were observed with field emission scanning electron microscopy (FESEM, Hitachi S-4800, Tokyo, Japan). Transmission electron microscope (TEM, JEM-2100; JEOL, Tokyo, Japan) was used to evaluate the internal structure of antiPD-L1-SPIOs@PLGA@Au and verify the corresponding elements with attached energy-dispersive X-ray spectroscopy (EDS). The size distribution and zeta potential of antiPD-L1-SPIOs@PLGA@Au were characterized using dynamic laser scattering (DLS) instrument (Zetasizer Nano ZS3690; Malvern Instruments, Malvern, UK).

Cell culture

B16F10 and HUVECs (Human Umbilical Vein Endothelial Cells) cell line were purchased from the Institute of Biochemistry and Cell Biology (Shanghai, China) and were cultured at 37 ℃ in DMEM (Clonogenic survival Gibco Life Technologies, Grand Island, NY, USA) containing 10% fetal bovine serum (FBS) and 1% penicillin–streptomycin at 37℃ in a humidified incubator containing 5% CO_2.

Murine tumor model

Mouse studies were performed in compliance with approval from the Division of Laboratory Animal Resources at the University of Fudan. Female, 6–8 weeks old, C57BL/6 mice were inoculated with B16F10 cells (2×10^5 B16F10) subcutaneously at the right flank. Tumors were allowed to grow until their volume was approximately 100 mm^3. Tumor volume was calculated using the formula: major axis ×(minor axis)^2×0.5. Mice were killed when tumors volume reached 3000 mm^3 or if the tumors ulcerated

In vitro cytotoxicity assessment

To evaluate the in vitro cytotoxicity of antiPD-L1-SPIOs@PLGA@Au, cell counting kit-8(CCK8) proliferation assay kit (Dojindo Molecular Technologies Inc., Japan) were performed at 12h and 24h after incubation. B16F10 cells and HUVECs at a density of 1×10^4/well in 96-well plates were treated with antiPD-L1-SPIOs@PLGA@Au at different concentrations (0, 10, 20, 50, 100, and 200μg/mL). The cells were incubated at 37℃ for 4 h, washed with PBS and further incubated for 12 h and 24 h. Then, the culture medium was replaced with CCK-8 solution (100 mL, containing 10% CCK-8) for additional 1 h, and the cell viability was detected by amicroplate reader (Thermo scientific Multiskan MK3) at the wavelength of 450 nm.

In vivo toxicity study

Female, 6–8 weeks old, C57BL/6 mice were injected with antiPD-L1-SPIOs@PLGA@Au (200 μl, 7 mg/ml). Toxicity of antiPD-L1-SPIOs@PLGA@Au in mice were observed 7 days post injection. Blood samples collected from the ophthalmic vein under anesthesia were used to test blood biochemistry indexes. Major organs including heart, liver, spleen, lung, and kidney were stained with hematoxylin and eosin (H&E), and the toxicity of nanoparticles was evaluated through observing the structure of major organs. Mice treated with saline was used as control group.

Targeting Specificity in vitro

B16F10 cells were seeded in confocal cell-culture dishes at a density of $2*10^4$ cells/well. FITC labelled antiPD-L1-SPIOs@PLGA@Au was added and incubated for 4 h. In the antibody blocking group, 5μl PD-L1 antibody without FITC was used to block PD-L1 before adding FITC labelled antiPD-L1-SPIOs@PLGA@Au. After washed three times with PBS, the cells were fixed with 4% paraformaldehyde for 15 min. Cell nuclei was stained with nucleus staining agent (DAPI; Beyotime Biotechnology Co., Ltd., Shanghai, China) for 10 min. Finally, the qualitative observation of samples were done under a confocal laser scanning microscopy (CLSM) (Leica TCS SP5 II, Leica Microsystems Ltd.,Mannheim, Germany).

Magnetic resonance imaging

AntiPD-L1-SPIOs@PLGA@Au was diluted in deionized water to various Fe concentrations (0, 0.002, 0.004, 0.006, and 0.008mM). MR imaging and relaxivity measurements were conducted with a 0.5 T MRI scanner (MiniMR-60, Shanghai Niumag Corporation). T2-weighted MR imaging of the samples was carried out using traditional spin-echo sequence, and the parameters were as follows: TR 2000 ms, TE 100 ms, slice thickness=3mm. Relaxivity (r2) was obtained from the fitting plots of 1/T2 (s^{-1}) versus Fe concentration (mM).

B16F10-bearing mice were classified into three groups. The first group was injected with antiPD-L1-SPIOs@PLGA@Au, the second group with SPIOs@PLGA@Au and the control group with saline. In vivo, tumor-bearing mice were imaged before and at different time points (0.5 h, 1 h, 2 h, 4 h, 6 h) after injection with antiPD-L1-SPIOs@PLGA@Au (200 μL, 7 mg/mL). MRI was performed using a Bruker 7.0T MRI scanner (BIOSPEC70/20USR, Germany). T2-weighted imaging parameters were TR 3000ms, TE 30ms, slice thickness= 1.0 mm.

Radiosensitization of melanoma cells with antiPD-L1-SPIOs@PLGA@Au.

The effectiveness of the combination of nanoparticles and ionizing radiation was assessed by clonogenic assays. B16F10 cells were incubated with SPIOs@PLGA@Au and antiPD-L1-SPIOs@PLGA@Au for 24 h. Cells were irradiated at different doses with 220 kV X-ray at a dose rate of 2 Gy/min using the Small Animal Radiation Research Platform (SARRP) at the Fudan University Shanghai Cancer Center. After irradiation, cells were trypsinized and counted. Known numbers were then replated

and returned to the incubator to allow macroscopic colony development. Colonies were counted after 7 days, and the plating efficiency and surviving fraction for given treatments were calculated. The mean lethal dose (Do), survival fraction (SF2) and SF2 sensitized ratio of B16F10 cells in different treatment groups were calculated by fitting the cell survival curve with multi target single hit equation: SF=1-(1-exp(D /D0))^N.

Therapeutic efficacy and survival study in B16F10-tumor-bearing mice

Mice were anesthetized intraperitoneally with 1 ml/kg of a solution containing 13 mg of ketamine and 86 mg of xylazine per ml. Mice were randomly divided into four groups composed of 4 mice each: saline, RT alone, RT plus SPIOs@PLGA@Au and RT plus antiPD-L1-SPIOs@PLGA@Au. Animals treated with SPIOs@PLGA@Au and antiPD-L1-SPIOs@PLGA@Au (200 μL, 7 mg/mL, IV injection) were exposed to radiation at the time point determined by findings of MRI. The total dose of 15 Gy was given in 1 fraction. After the treatments, the tumor size and body weight were recorded every 2 days.

ROS measurement in vitro.

Cells were seeded in triplicate in 12-well plates 24 h prior to treatment, pretreated with SPIOs@PLGA@Au or antiPD-L1-SPIOs@PLGA@Au for 24 h, and then irradiated. After irradiation, fresh medium containing 4 μM CM-H2DCFDA (ThermoFisher, C6827) for ROS measurements was added to each well. After incubation for 30 min in a humidified incubator (at 37 ° C, 5% CO2), the cells were washed with PBS and trypsinized to obtain a cell suspension. ROS was analyzed by Bio-Rad microplate reader (Biotek Synergy 4) at 488 nm or visualized by CLSM.

γ-H2AX formation experiment

B16F10 cells were cultured in a confocal culture dish with inoculation density of 5×10^4. After 24 hours of culture, the cells were divided into 3 groups: radiation aline group, SPIOs@PLGA@Au combined radiation group and antiPD-L1-SPIOs@PLGA@Au combined radiation group, with 3 replicated holes in each group. The concentrations of SPIOs@PLGA@Au and antiPD-L1-SPIOs@PLGA@Au were 200μg/ ml. The cells were irradiated with 220KV X-ray at a single dose of 6Gy. Twenty-four hours after irradiation, paraformaldehyde fixative was added and fixed for 10-15 minutes. Anti- phosphorylated histone γ-H2AX monoclonal antibody was incubated overnight in a wet box at 4℃. Diluted CY3-labeled sheep anti-mouse secondary antibody (1:1000) was used as second antibody. The number of fluorescence bright spots in at least 50 cells in each field was counted under the microscope.

In vitro evaluation of the effect on the polarization of macrophages

We used macrophages derived from mouse bone marrow mesenchymal stem cells stimulated by M-CSF differentiation. A transwells two-compartment petri dish system with an interseptal aperture of 0.4 micron was used. In this dish, molecules can pass freely through membrane pores, but cells cannot. Mouse macrophages were cultured in the lower chamber and upper chamber were divided into 4 groups: PBS

group, tumor cell B16F10 group, tumor cell B16F10+SPIOs@PLGA@Au mixed solution group and tumor cell B16F10+antiPD-L1-SPIOs@PLGA@Au mixed solution group. After 24 h co-culture, macrophages in the lower chamber were isolated and the difference in the number of CD86-positive (M1 type) and CD206-positive (M2 type) macrophages was analyzed by flow cytometry.

Immunofluorescence assay

To characterize the TAMs polarization markers(F4/80, CD 86 and CD 206), the infiltration of CD4+ and CD8+ T cells the expression of CRT in tumor section, immunofluorescence assays were performed. Frozen tissue sections of 6 mm thickness were prepared, air-dried for at least 1 h and then fixed in acetone for 10 min at -20 ℃. After blocking with 20% donkey serum, the sections were incubated with primary antibodies overnight at 4 ℃, followed by incubation with dye-conjugated secondary antibodies for 1 h. After staining with DAPI for another 10 min, the sections were then washed twice with PBS and observed under CLSM (Olympus, IX83).

Flow cytometry

Cells were stained with the following fluorochrome-conjugated antibodies: CD3, CD4, CD8, F4/80, CD86 and CD206, and then tested by flow cytometry. Data analysis was carried out using FlowJo software.

Enzyme-linked immunosorbent assay ELISA

The sera of mice in each treatment group were collected from the ophthalmic vein 7 days after treatment and assayed for mouse interferon-γ (IFN-γ), tumor necrosis factor α (TNF-α), and interleukin 12 (IL-12) levels using quantitative enzyme-linked immunosorbent assay kit, following validation of each ELISA according to the manufacturer's instructions. Absorbance was read using a Bio-Rad microplate reader (Biotek Synergy 4) at 488 nm.

Statistical analysis

All in vitro experiments were carried out in triplicate. Data were expressed as the mean ± standard error (SE). Comparison between two groups was performed using an unpaired two-tailed t-test. When comparing multiple groups, a one-way analysis of variance (ANOVA) were used. Kaplan–Meier survival curves were analysed using the log-rank test for the survival data. Differences were considered statistically significant when $P < 0.05$.

Results

Characterizations of antiPD-L1-SPIOs@PLGA@Au

Using an oil-in-water emulsion method, SPIOs@PLGA was prepared with a mean hydrodynamic diameter of 200 nm and low polydispersity (PDI <0.25) as determined by dynamic light scattering. SPIOs@PLGA exhibited well-defined spherical shape and homogenous sizes (Figure 1A-C). TEM image illustrated the

deep gray spots in the shell and core region of the nanoparticle, indicating that SPIOs were encapsulated in the PLGA matrix. SPIOs@PLGA was negatively charged with a zeta potential of approximately –18.8mV, which could be used to absorb positively charged PAH so as to subsequently attach negatively charged citrate estabilized Au NPs. Au NPs were coated on the surface of SPIOs@PLGA through electrostatic adsorption. Afterward, the attached Au NPs with an average size of 5–7nm were served as seeds to nucleate the growth of an Au nanoshells around SPIOs@PLGA by a seeding procedure. SEM image illustrated (Figure 1D) that the regular spherical morphology was well maintained but the surface roughness increased due to deposition of aggregated Au NPs. As TEM image (Figure 1E) clearly illustrated, dense Au nanoparticles were distributed homogeneously on the surfaces of PLGA to form Au nanoshells. EDS elements mapping (Figure 1(F-I)) of SPIOs@PLGA@Au clearly revealed the presence of characteristic C, Fe, Au and O elements□F:C□G:Fe□H:Au□I:O□

To synthesize antiPD-L1-SPIOS@PLGA@Au, SH–PEG–COOH was linked to SPIOs@PLGA@Au via Au–S linkage and then anti-PD-L1 antibody was coupled with PEG chain via an amide linkage catalyzed by EDC/NHS method. The average size of antiPD-L1-SPIOS@PLGA@Au NCs was 280.6 nm with a polydispersity index of 0.14(Figure 1J), and zeta potential was about –24.2mV, which indicated the good solution stability of it. Notably, antiPD-L1-SPIOs@PLGA@Au were highly stable in storage (PBS, 4 °C) for at least 7 days, with no apparent change in the median hydrodynamic diameter or size distribution, as determined by DLS. We observed with a confocal laser scanning microscopy that the FITC-labeled antibody of antiPD-L1-SPIOS@PLGA@Au was successfully connected (Figure 2).

The morphology of antiPD-L1-SPIOs@PLGA@Au stayed stable. And radiation of 6Gy could cause the rupture of Au shell. The Au shell was break into smaller Au debris and the inside SPIOs would be released (Figure S1).

The cytotoxicity of antiPD-L1-SPIOs@PLGA@Au

We used CCK-8 assay to investigate the cytotoxicity of antiPD-L1-SPIOs@PLGA@Au on B16F10 cells and HUVECs. As shown in Figure 3, the cell viability of B16F10 cells and HUVECs remained more than 85% after incubation with antiPD-L1-SPIOs@PLGA@Au, even at the highest concentration (200 μg/ml) for 24 h.

To further investigate in vivo toxicity profile, antiPD-L1-SPIOs@PLGA@Au was injected intravenously via tail of C57BL/6 mouse. Blood samples were taken from the eyes of mice at 7 day after injection to test the blood biochemical including myocardial enzyme spectrum, liver function and renal function. All measured parameters were normal, indicating that antiPD-L1-SPIOs@PLGA@Au would not induce significant systemic side effects to mice (Figure 4A). The histopathology of the heart, lung, liver, spleen and kidney was analyzed to assess the biosafety of nanoparticles. The nanoparticles showed no substantial damage to the major organs (Figure 4B), as evidenced by the stable body weights and lack of histopathological changes in major organs. This illustrated the good biocompatibility of antiPD-L1-SPIOs@PLGA@Au, which is an essential pre-requisite for imaging and radiosensitizing applications.

During the whole observation period, there was no significant difference in body weight among different groups (Figure 8D).

Targeting of antiPD-L1-SPIOs@PLGA@Au to B16F10 cells

To detect the targeting of the antiPD-L1-SPIOs@PLGA@Au to B16F10 cells that highly expressed the PD-L1 (Figure S2), the localization of antiPD-L1-SPIOs@PLGA@Au was visualized by direct observation under a fluorescent microscopy. It's demonstrated that after 4 h of incubation, antiPD-L1-SPIOs@PLGA@Au could be detected on the cell membrane, where PD-L1 expressed in B16F10 cells. As can be seen from the bright field images, antiPD-L1-SPIOs@PLGA@Au, which aggregated into ink spots, were mainly distributed in the cell membrane and cytoplasm. In image of FITC pathway, green fluorescence signal was observed on the ink spots (Figure 5).

Through blocking with anti-PD-L1 antibody unlabeled with FITC, the connection between nanomaterials and B16F10 cells was significantly reduced after rinsing with PBS. No obvious ink spot and fluorescent-labeled antibody was observed on the bright field image and FITC channel (Figure 5), suggesting that antibody-mediated active targeting linking played an important role in the binding of targeted nanoparticles to B16F10 cells.

MR imaging in vitro/vivo

T_2-weighted imaging of antiPD-L1-SPIOs@PLGA@Au was performed with different Fe concentrations under a 0.5 T magnetic field. The transverse relaxation rate ($1/T_2$) of antiPD-L1-SPIOs@PLGA@Au aqueous solution as a function of iron concentration are shown in Figure 6A. According to the fitting curve, the T_2 relaxivity (r2) of antiPD-L1-SPIOs@PLGA@Au aqueous solution was calculated to be 286.24 mM^{-1} s^{-1}, higher than that of the commercially available MRI contrast agent.

T_2 weighted images were obtained at pre-injection and 0.5h, 1h, 2h, 4h, 6h after injection (200μl, 7mg/ml) using a Bruker BIOSPEC70/20USR 7.0T MRI scanner. Nanoparticles contrast showed gradual enrichment and then regressed in the tumor site. The best enhancement effect in tumor was at the second hour after intravenous injection of antiPD-L1-SPIOs@PLGA@Au and SPIOs@PLGA@Au (Figure 6B and 6C). However, tumor in the targeted nanoparticle group is still hypointense on MRI until 6h, with higher $1/T_2$ value than that in non-targeted group, reflecting the ability to target to PD-L1. In contrast, there was no significant changes of signal in tumor in saline group.

AntiPD-L1-SPIOs@PLGA@Au enhancing radiosensitivity of B16F10 melanoma.

In vitro

Compared with radiation alone, SPIOs@PLGA@Au or antiPD-L1-SPIOs@PLGA@Au combined radiation significantly reduced the rate of clone formation of B16F10 cells (Figure 6A) in terms of the number of colony formation and the fitted survival curve. The mean lethal dose (Do) of radiation alone,

SPIOs@PLGA@Au combined radiation group and antiPD-L1-SPIOs@PLGA@Au combined radiation group were 1.93Gy, 1.51Gy and 1.34Gy, respectively. The Do sensitization ratios of the SPIOs@PLGA@Au and antiPD-L1-SPIOs@PLGA@Au groups were 1.5 and 1.34, respectively, while the SF2 sensitization ratios were 1.26 and 1.4 (Table 1).

In vivo

Based on the results of in vivo imaging monitoring, irradiation was given at 2h after intravenous injection. Compared with the saline group, the tumor growth in the mice given with radiation alone was temporarily slowed down, but accelerated 8 days after radiation. The tumor inhibition effects of radiation combined with SPIOs@PLGA@Au or antiPD-L1-SPIOs@PLGA@Au was higher than that of radiation alone. Within 12 days after irradiation, tumor inhibition was similar between SPIOs@PLGA@Au group and antiPD-L1-SPIOs@PLGA@Au group, but 12 days after irradiation, tumor growth accelerated in SPIOs@PLGA@Au group. However, the tumor inhibition effect of antiPD-L1-SPIOs@PLGA@Au lasted until 22 days, and no obvious acceleration of tumor growth was observed (Figure 8A). TUNEL staining showed more apoptosis in the antiPD-L1-SPIOs@PLGA@Au group. HE staining sections revealed that there were large necrotic foci of tumor tissue in the antiPD-L1-SPIOs@PLGA@Au group (Figure 8B).During the entire observation period, only the mice in the antiPD-L1-SPIOs@PLGA@Au group did not die that lived for more than 3 weeks. The Kaplan–Meier survival curves of the treated groups are illustrated in Figure 8C. During the whole observation period, there was no significant difference in body weight among all groups (Figure 8D).

The mechanism of antiPD-L1-SPIOS@PLGA@Au for enhancing treatment efficacy

Reactive oxygen species (ROS)

ROS formation and resulting oxidative stress reaction is an important mechanism for inorganic nanomaterials sensitizing radiation. It was found in DCFH-DA assay that more ROS formation was observed when either antiPD-L1-SPIOs@PLGA@Au or SPIOs@PLGA@Au were applied, compared with radiation alone (Figure 5 A). The amount of ROS produced by antiPD-L1-SPIOs@PLGA@Au and RT was the highest among the groups (Figure 5 B).

DNA repair

When DNA double strand breaks, histone H2AX will be directly activated, causing the rapid phosphorylation of histone H2AX to form γ-H2AX. Under fluorescence microscope, the number of foci of γ -H2Ax increased mildly in the radiation alone group, while in SPIOs@PLGA@Au+RT combined radiation group and antiPD-L1-SPIOs@PLGA@Au combined radiation group, there were more γ -H2Ax foci. The fluorescence intensity of the antiPD-L1-SPIOs@PLGA@Au combined radiation group was the strongest (Figure 10).Counting results showed that the average focal number of γ-H2AX in the SPIOs@PLGA@Au+RT and antiPD-L1-SPIOs@PLGA@Au+RT groups was 1.68 times and 1.84 times higher than that in the control group ($P<0.05$).

Re-polarization effects on macrophages

In transwell dish, macrophages in lower compartment were co-cultured with different upper compartment culture medium in different group. The expression of CD86 (M1 type) and CD206 (M2 type) in macrophages was detected by flow cytometry. The results (Figure 11) showed that the expression rates of CD86 and CD206 in macrophages in PBS group were similar. After co-culture with B16F10 alone, a large amount of CD206 was expressed, indicating that tumor cells can transform macrophages into tumor growth-promoting M2 type. After adding SPIOs@PLGA@Au or antiPD-L1-SPIOs@PLGA@Au with B16F10, M1 type macrophages expressing CD86 increased significantly, while M2 type macrophages expressing CD206 decreased significantly, indicating that nanoparticles consisting of Au and SPIOs have the function of reversing TAMs. However, no significant difference in the re-polarization effect between PD-L1 targeted nanoparticles and non-targeted nanoparticles, indicating that the reverse effect on TAMs is mainly caused by Au-SPIOs nanoparticles, while PD-L1 has no significant effect on TMAs polarization.

Furthermore, we verified the effect of nanomaterials on TAMs polarization in the murine subcutaneous B16F10 model. The tumor bearing mice were randomly divided into four groups: saline group, radiation alone group, SPIOs@PLGA@Au combined radiation group and antiPD-L1-SPIOs@PLGA@Au combined radiation group. One week after different treatments, the expression of CD206, CD86 and F4/80 proteins in the tumor tissue was detected by immunofluorescence staining. The results showed that F4/80 expression, representing the total number of macrophages, had no significant difference among the four different treatment groups. However compared with the saline group and the radiation alone group, the expression of CD86 increased significantly in the SPIOs@PLGA@Au and antiPD-L1-SPIOs@PLGA@Au groups, while the expression of CD206 decreased (Figure 12).Moreover, targeted nanomaterials have a stronger ability to transform TAMs into M1 than the non-targeted group. This result is different from the in vitro experiment, which may be explained by that targeted nanomaterials enable more Au-SPIOs nanomaterials to actively target into tumor tissues and obtain a higher concentration, thus achieving a better re-polarizaiton effect.

The expression of calreticulin (CRT)

Radiotherapy induces immunogenic cell death characterized by high expression of calreticulin (CRT) on the surface of dying cancer cells, thereby inducing effective immune responses. We studied the expression of CRT on the surface of cancer cells 7 days after different treatments by immunofluorescence stain and Western blot analysis. Both antiPD-L1-SPIOs@PLGA@Au and SPIOs@PLGA@Au combined with RT resulted in a higher expression of CRT compared to RT alone. The highest expression of CRT was observed in antiPD-L1-SPIOs@PLGA@Au group (Figure 13).

Infiltration of $CD4^+$ and $CD8^+$ T cell in tumor

To evaluate the activation of tumor-specific immunity induced by antiPD-L1-SPIOs@PLGA@Au, T cells in tumor section were assessed by immunofluorescence staining analysis. In the saline group, no obvious infiltration of $CD4^+$ and $CD8^+$ T cell in the tumor tissues was observed. Both radiation alone and radiation

combined with SPIOs@PLGA@Au increased the level of $CD4^+$ and $CD8^+$ T cell. The highest level of CD8 and the ratio of CD8/CD4 were achieved in radiation combined with antiPD-L1-SPIOs@PLGA@Au group, suggesting more infiltration of activated CD8+T cell (Figure 14).

The activating of anti-tumor immune response

Moreover, to better understand how antiPD-L1-SPIOs@PLGA@Au with radiation interact with immunological system, we harvested tumor draining lymph nodes for analyzing the proliferation of T cell, and the sera of mice one week after different treatments was collected to analyze IFN-γ, TNF-α and IL-12 level by ELISA. CD8+ T cell significantly increased in the presence of antiPD-L1-SPIOs@PLGA@Au compared with SPIOs@PLGA@Au, and the ratio of CD8/CD4 was higher in antiPD-L1-SPIOs@PLGA@Au group than that in the SPIOs@PLGA@Au group (Figure 15).

In control group, Il-12 decreased one week after injection of saline, while IFN-γ and TNF-α did not change significantly. IFN-γ and TNF-α were slightly increased in the radiation alone group, but there was no statistical significance. IFN-γ and IL-12 in the untargeted nanoparticles group showed a statistically significant increase. IFN-γ, TNF-α and IL-12 were significantly increased in the antiPD-L1-SPIOs@PLGA@Au group, indicating that the targeted nanomaterials have a significant activation effect on the immune response (Figure 16).

Discussion

Radiation therapy is employed extensively for treatment of almost all types of solid tumors. Unfortunately, ionizing radiations do not discriminate between cancerous and normal cells. Thus, normal tissue damage is still the dose limiting factor that diminishes tumor cells eradication in radiation therapy. Application of tumor-specific nanoparticles in radiation therapy has aimed to improve the radiation therapy outcomes by inducing more toxicity for tumors and less for normal tissue. On the other hand, the tumoricidal effects of RT are in part dependent on an intact immune system. Radiation leads to an increased release of tumor antigens, cytokines and chemokines which promotes tumor specific T cell trafficking and priming. Unfortunately, like a double-edged sword, radiation can also create an immunosuppressive environment. Radiation resulted in upregulation of PD-L1 expression, which exhausts the number of T cells and impaired antitumor immunity [11]. To address the aforementioned obstacle to improve the radiation effects, we fabricated PD-L1-targeted multifunctional nanoplatform, in which Au was coated on the surface of PLGA encapsulated with SPIOs to enhance radiosensitization of the melanoma and switch microenvironment immunosuppressive to immunoreactive. With the addition of antiPD-L1-SPIOS@PLGA@Au, the survival of melanoma-bearing mice was significantly prolonged. All the mice survived for 20 days after the combination therapy of antiPD-L1-SPIOs@PLGA@Au and radiation. These results indicate that the combination of antiPD-L1-SPIOs@PLGA@Au and radiation strategy would be a promising approach to effective antitumor therapy.

Due to containing high Z-material Au with the property of high absorption and deposition of energy, antiPD-L1-SPIOs@PLGA@Au results in a SER of 1.4, which is comparable to that achieved by other Au formulations reported in the literature. The radiation enhancing effect can be increased with specific targeting to overexpressed receptor on the surface of tumor cell which can promoted the cellular uptake. A significantly higher dose enhancement effect was achieved with anti-PD-L1-conjugated (SER = 1.4) versus non-conjugated nanoparticle (SER = 1.26), which was attributed to higher cellular uptake of the targeted nanoparticles by B16F10 cells that express high level PD-L1.

For a long circulation of nanoparticles within the blood stream, it is favorable to have relatively larger size of the nanoparticles [12]. Targeted nanocapsules used in this study were designed to have average diameters of about 280nm, which can have low renal clearance, reduce the non-specific uptake by normal organ and prolong the circulation time. When they reached the tumor with acid microenvironment and was irradiated by X ray, Au nanoshell would break into about 10–100 nm Au bris, which are favorable for cellular uptake [13, 14]. Higher cellular uptake would result in higher radiosensitivity. AntiPD-L1-SPIOs@PLGA@Au combined RT in this study alleviated the dilemma between the circulation time and the cellular uptake.

AuNPs shell structure with cavity inside provide an ideal platform for multi-functional applications due to their unique morphological and optical properties. The nanocapule with Au shell not only enables radiosensitization, but the shell thickness can also be fine-tuned for photothermal ablation using near infrared ray (NIR). As well, the hollow cavity can be utilized to encapsulate high loading of therapeutic agents and image contrast. Park et al. evaluated the therapeutic of DOX-loaded hollow AuNPs for combining chemo-, radio- and thermal therapy [15]. The triple combination group was shown to result in a 4.3-fold increase in tumor growth delay, as well as a 6.8-fold reduction in tumor weight. In this study we encapsulated SPIOs for highly sensitive MR imaging. The tumor accumulation of antiPD-L1-SPIOS@PLGA@Au generated a hypointensive signal in MRI, addressing low sensitivity of Au a CT contrast agent, which requires delivery of significantly higher concentrations of Au to the tumor to generate sufficient contrast enhancement in CT (mM range) relative to the amount necessary for radiosensitization (μM range). Besides contrast for MRI, SPIOs have magnetic property. Magnetic core of the nanocomplex allowed in vivo magnetic navigation to improve tumor targeting and minimize off-target effect[16].

Immune checkpoint inhibitors (ICIs) targeting PD-1, PD-L1 and CTLA-4 can relieve the tumor restraint of anti-tumor T cell immunity and improve the prognosis of patients with advanced cancer [17]. However, the curative effect of ICIs depends on the T cells activation. Immunosuppressive cells contributing to the immune evasion will lead to the failure of ICIs [18]. Therefore, how to inhibit the activity of these immunosuppressive cells is currently a matter of concern, among which TAM is one of the typical immunosuppressive cells that occupies a significant part of tumor mass [19, 20, 21]. TAMs were able to inhibit the mature of antigen present cells (APCs) and CD8 + T cell-mediated anti-tumor immune responses by producing high levels of IL-10[22, 23]. Recently, SPIOs were found to be able modulate immune microenvironment. It was shown to SPIOs polarized tumor-associated macrophages from a

protumor M2-like to an antitumor M1-like phenotype, which releases reactive oxygen species to induce tumor cell killing [5, 24]. In this study, treating with SPIOs-containing nanoparticle significantly elevated the expression of CD86 and reduced the expression of CD206 compared to RT alone, indicating the polarization to M1.

Moreover, it's demonstrates that macrophages are the predominant immune cells that express PD-L1 [25, 26]. These PD-L1 + TAMs could mediate CD8 + T cell dysfunction via the PD-1/PD-L1 interaction. TAMs have been regarded as carriers of checkpoint ligands that are upregulated in response to TME-derived factors, resulting in immune exhaustion via the checkpoint ligand/receptor interaction in a cell-to-cell contact manner. Therefore, the blocking effect of ICIs on the checkpoint molecules expressed on TAMs is increasingly attracting attention [27]. AntiPD-L1-SPIOs@PLGA@Au realized dual-targeting strategy, achieving the combination of reprogramming and elimination of TAM and inhibition of immune checkpoint. AntiPD-L1-SPIOs@PLGA@Au with local RT not only increased the number of $CD8^+$ cells in tumor but also enhance the proliferation of $CD8^+$ cells in the tumor draining lymph nodes (TDLN) and elevate the level of serum IFN, indicating the activation of systemic antitumor immunity. A further understanding of their intracellular regulatory mechanisms will be helpful for precise application of TAMs targeted therapy and ICI treatment.

Conclusions

We successfully prepared antiPD-L1-SPIOs@PLGA@Au nanoparticles, which realized the combination of radiotherapy and immunotherapy and enhance the antitumor effect. With the application of antiPD-L1-SPIOs@PLGA@Au, we enabled to target the PD-L1, increase the accumulated concentration of nanoparticle in tumor and enhance B16F10 sensitivity to radiation. By inducing the repolarization from M2 type to M1 and elevating the expression of CRT, antiPD-L1-SPIOs@PLGA@Au was able to switch the immunosuppressive environment. Combined with the effect of blocking the PD-1/PD-L1 checkpoint pathway, antiPD-L1-SPIOs@PLGA@Au and RT activated the tumor specific immunity ultimately. These results indicate that the combination of antiPD-L1-SPIOS@PLGA@Au and RT strategy would be a promising approach to effective antitumor therapy.

Abbreviations

Au NPs: Gold Nanoparticles; B16F10: Mouse melanoma cell line B16F10; CCK-8: Cell Counting Kit-8; CK-MB: Creatine Kinase-MB; CD3e: Cluster of Differentiation3e; CD4 : Cluster of Differentiation4 CD8: Cluster of Differentiation8; CD86: Cluster of Differentiation86; CD206: Cluster of Differentiation206 CRT: calreticulin; DLS : Dynamic Laser Scattering; EDC: Ethyl-3-(3-dimethylami-nopropyl) Carbondiimine; EDTA : Ethylenediaminetetraacetic Acid FCM: Flow Cytometry FBS: Fetal Bovine Serum; FE-SEM: Field Emission Scanning Electron Microscopy FITC: Fluorescenin isothiocyanate; HUVEC: Human Umbilical Vein Endothelial Cells; ICD: immunogenic cell death; IFN-γ: Interferon gamma IL-12: Interleukin-10; LDH: Lactate Dehydrogenase; MRI : Magnetic Resonance Imaging; NPs: Nanoparticles; NHS: N-Hydroxysuccinimide; PAH : Poly ally Amine Hydrochloride; PBS:Phosphate Buffer Saline; PLGA:

Poly(lactic-co-glycolic acid); PVA : Polyvinyl Alcohol; PD-1: programmed cell death; PD-L1: programmed cell death-Ligand 1; SH-PEG-COOH: Thiol, carboxyl-terminated poly(ethylene glycol); TAMs: tumor associated macrophages; TNF-α: Tumor Nercrosis Factor-α TGF-β: Transforming Growth Factor-β

Declarations

Ethics approval and consent to participate

Mouse studies were performed in compliance with approval from the Division of Laboratory Animal Resources at the University of Fudan.

Consent for publication

All authors gave their consent for publication.

Availability of data and materials

The datasets generated and analyzed during the current study are included

in this article.

Competing interests

The authors declare that they have no competing interests

Funding

This research is supported by Shanghai Anticancer Association EYAS PROJECT (SACA-CY19C11)

Authors' Contributions

CD, CW, CH and HY conceived and designed the study. CD, JJ and GP synthesized and characterized the antiPD-L1-SPIOs@PLGA@Au. CD, CW, JJ, and GP carried out the cell-based assays and animal experiments. All authors contributed to the analysis and interpretation of the data. CD, JJ and CW wrote the manuscript. CH and HY revised the manuscript. All authors read and approved the final manuscript.

Acknowledgements

We appreciate Yun Deng for the help in the in vivo study and data collecting.

References

1. Delaney G, Jacob S, Featherstone C, Barton M. The role of radiotherapy in cancer treatment: estimating optimal utilization from a review of evidence-based clinical guidelines. Cancer. 2005;104(6):1129–1137.

2. Her S, Jaffray DA, Allen C. Gold nanoparticles for applications in cancer radiotherapy: Mechanisms and recent advancements. Adv Drug Deliv Rev. 2017;109:84–101.
3. Bulte JW, Kraitchman DL. Iron oxide MR contrast agents for molecular and cellular imaging. NMR Biomed. 2004;17(7):484–499.
4. McQuade C, Al Zaki A, Desai Y, et al. A multifunctional nanoplatform for imaging, radiotherapy, and the prediction of therapeutic response. Small. 2015;11(7):834–843..
5. Zanganeh S, Hutter G, Spitler R, et al. Iron oxide nanoparticles inhibit tumour growth by inducing pro-inflammatory macrophage polarization in tumour tissues. Nat Nanotechnol. 2016;11(11):986–994.
6. Wang Y, Wang H, Yao H, Li C, Fang JY, Xu J. Regulation of PD-L1: Emerging Routes for Targeting Tumor Immune Evasion. Front Pharmacol. 2018;9:536.
7. Qu QX, Xie F, Huang Q, Zhang XG. Membranous and Cytoplasmic Expression of PD-L1 in Ovarian Cancer Cells. Cell Physiol Biochem. 2017;43(5):1893–1906.
8. Topalian SL, Drake CG, Pardoll DM. Immune checkpoint blockade: a common denominator approach to cancer therapy. Cancer Cell. 2015;27(4):450–461.
9. Karam SD, Raben D. Radioimmunotherapy for the treatment of head and neck cancer. Lancet Oncol. 2019;20(8):e404-e416.
10. Zheng D, Wan C, Yang H, et al. Her2-Targeted Multifunctional Nano-Theranostic Platform Mediates Tumor Microenvironment Remodeling and Immune Activation for Breast Cancer Treatment. Int J Nanomedicine. 2020;15:10007–10028.
11. Kikuchi M, Clump DA, Srivastava RM, et al. Preclinical immunoPET/CT imaging using Zr-89-labeled anti-PD-L1 monoclonal antibody for assessing radiation-induced PD-L1 upregulation in head and neck cancer and melanoma. Oncoimmunology. 2017;6(7):e1329071.
12. Dreaden EC, Austin LA, Mackey MA, El-Sayed MA. Size matters: gold nanoparticles in targeted cancer drug delivery. Ther Deliv. 2012;3(4):457–478.
13. Huo S, Ma H, Huang K, et al. Superior penetration and retention behavior of 50 nm gold nanoparticles in tumors. Cancer Res. 2013;73(1):319–330.
14. Adair JH, Parette MP, Altinoglu EI, Kester M. Nanoparticulate alternatives for drug delivery. ACS Nano. 2010;4(9):4967–4970.
15. Park J, Park J, Ju EJ, et al. Multifunctional hollow gold nanoparticles designed for triple combination therapy and CT imaging. J Control Release. 2015;207:77–85.
16. Chiang CS, Lin YJ, Lee R, et al. Combination of fucoidan-based magnetic nanoparticles and immunomodulators enhances tumour-localized immunotherapy. Nat Nanotechnol. 2018;13(8):746–754.
17. Topalian SL, Hodi FS, Brahmer JR, et al. Safety, activity, and immune correlates of anti-PD-1 antibody in cancer. N Engl J Med. 2012;366(26):2443–2454.
18. Tumeh PC, Harview CL, Yearley JH, et al. PD-1 blockade induces responses by inhibiting adaptive immune resistance. Nature. 2014;515(7528):568–571.

19. Yang Q, Guo N, Zhou Y, Chen J, Wei Q, Han M. The role of tumor-associated macrophages (TAMs) in tumor progression and relevant advance in targeted therapy. Acta Pharm Sin B. 2020;10(11):2156–2170.
20. Meng Y, Beckett MA, Liang H, et al. Blockade of tumor necrosis factor alpha signaling in tumor-associated macrophages as a radiosensitizing strategy. Cancer Res. 2010;70(4):1534–1543.
21. Pollard JW. Tumour-educated macrophages promote tumour progression and metastasis. Nat Rev Cancer. 2004;4(1):71–78.
22. Kitamura T, Qian BZ, Pollard JW. Immune cell promotion of metastasis. Nat Rev Immunol. 2015;15(2):73–86.
23. Akalu YT, Rothlin CV, Ghosh S. TAM receptor tyrosine kinases as emerging targets of innate immune checkpoint blockade for cancer therapy. Immunol Rev. 2017;276(1):165–177.
24. Li K, Lu L, Xue C, et al. Polarization of tumor-associated macrophage phenotype via porous hollow iron nanoparticles for tumor immunotherapy in vivo. Nanoscale. 2020;12(1):130–144.
25. Wu K, Kryczek I, Chen L, Zou W, Welling TH. Kupffer cell suppression of CD8 + T cells in human hepatocellular carcinoma is mediated by B7-H1/programmed death-1 interactions. Cancer Res. 2009;69(20):8067–8075.
26. Kuang DM, Zhao Q, Peng C, et al. Activated monocytes in peritumoral stroma of hepatocellular carcinoma foster immune privilege and disease progression through PD-L1. J Exp Med. 2009;206(6):1327–1337.
27. Gordon SR, Maute RL, Dulken BW, et al. PD-1 expression by tumour-associated macrophages inhibits phagocytosis and tumour immunity. Nature. 2017;545(7655):495–499.

Figures

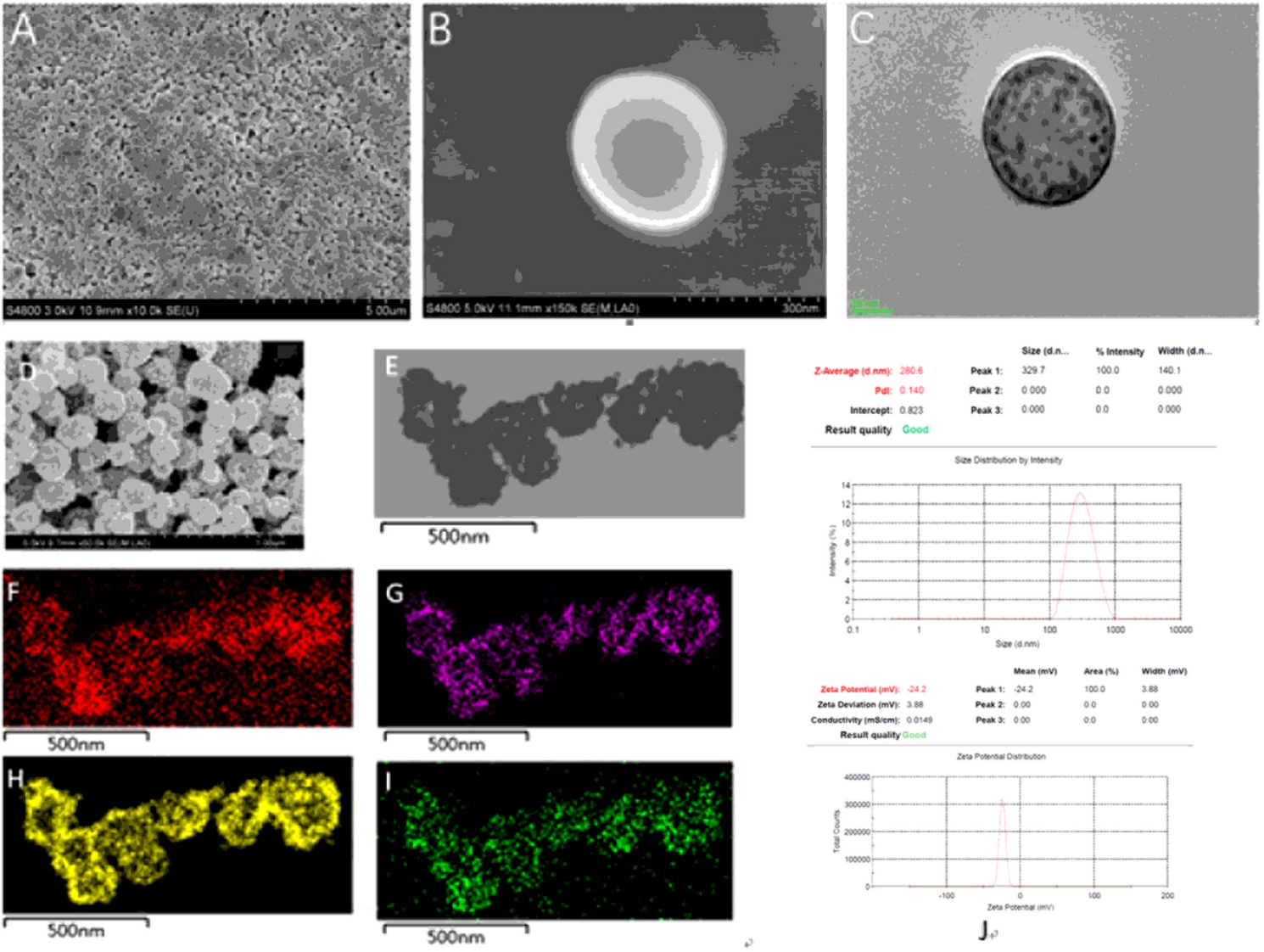

Figure 1

Characterizations of nanoparticles: (A) SEM (scale bar=5μm) image of SPIOs@PLGA; (B) SEM (scale bar=300nm) images of SPIOs@PLGA; (C) TEM images of SPIOs@PLGA; (D) SEM (scale bar=1μm) images of SPIOs@PLGA@Au; (E) TEM images of SPIOs@PLGA@Au; (F-I) EDS element mapping images of SPIOs@PLGA@Au exhibiting the presence of characteristic C, Fe, Au and O elements（F:C，G:Fe，H:Au，I:O）; (J) Average size and size distribution of antiPD-L1-SPIOs@PLGA@Au.

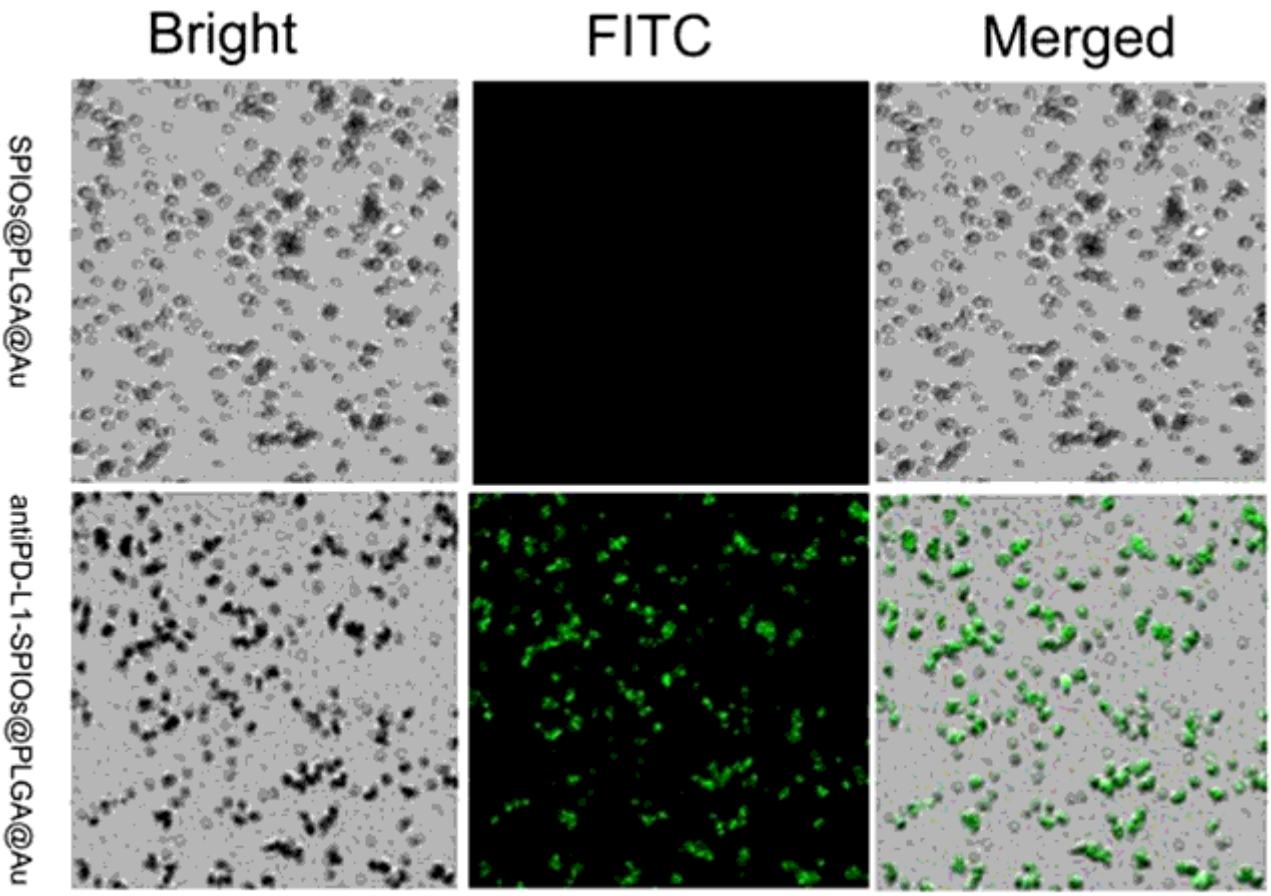

Figure 2

Confocal laser scanning microscopy images of SPIOs@PLGA@Au and antiPD-L1-SPIOs@PLGA@Au labelled with FITC.

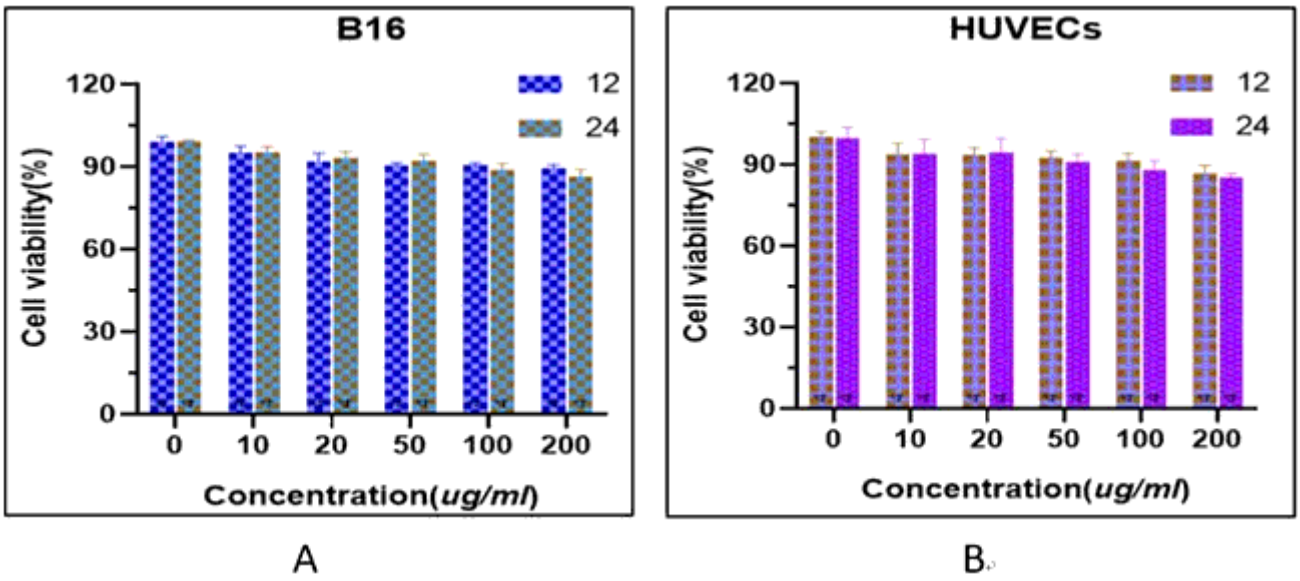

Figure 3

Cell viability of (A) B16F10 cell and (B) HUVECs after incubation (12h and 24h) with various concentrations of antiPD-L1-SPIO@PLGA@Au nanoparticles.

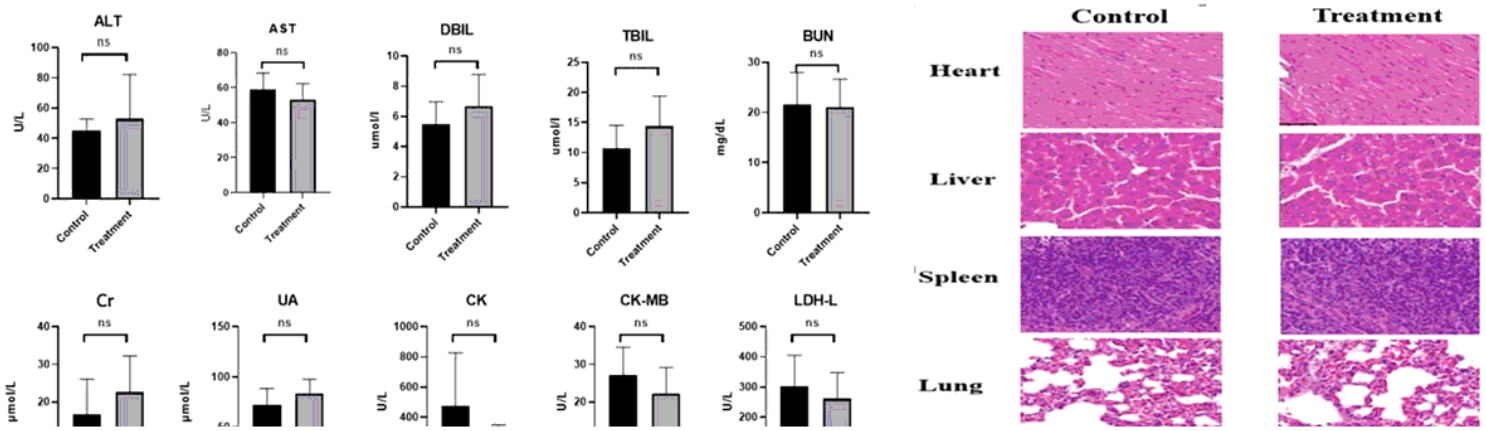

Figure 4

(A) The blood biochemistry of mice treated with antiPD-L1-SPIOs@PLGA@Au or saline (control). (B) Microscope images of H&E stained tissues in various organs including heart, liver, spleen, lung and kidney.

Figure 5

antiPD-L1-SPIOs@PLGA@Au targeting to B16F10 cell, with and without antiPD-L1 antibody blocking.

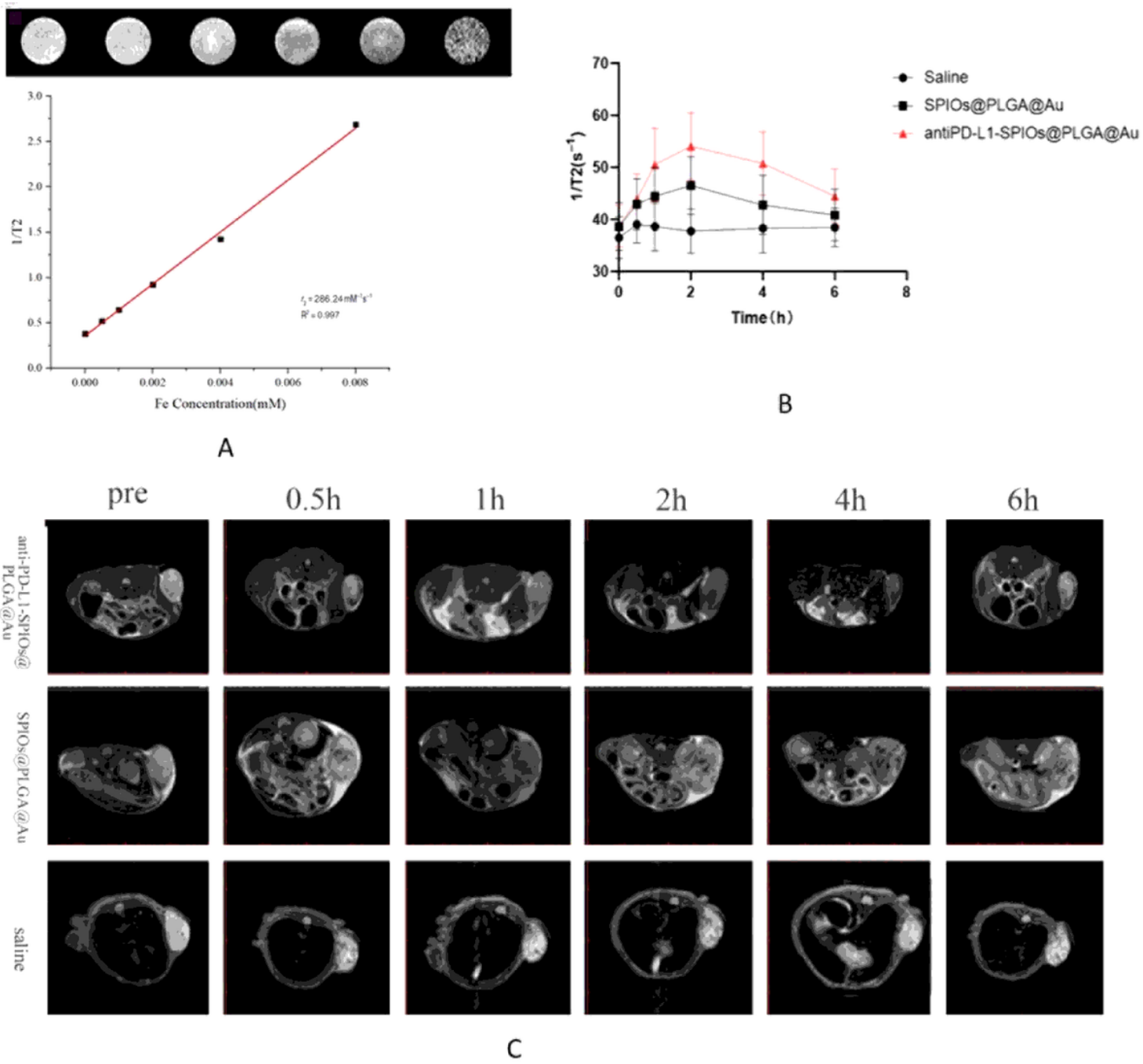

Figure 6

(A) T_2-weighted MR images of antiPD-L1-SPIOs@PLGA@Au with increasing Fe concentrations; (B) T_2 relaxation rate ($1/T_2$(s-1)) corresponding to region of interest of tumor at different time points (0h, 0.5h, 1h, 2h, 4h, 6h) with different injections. (C) T_2-weighted MR imaging of a B16F10 mice xenograft tumor at different time points.

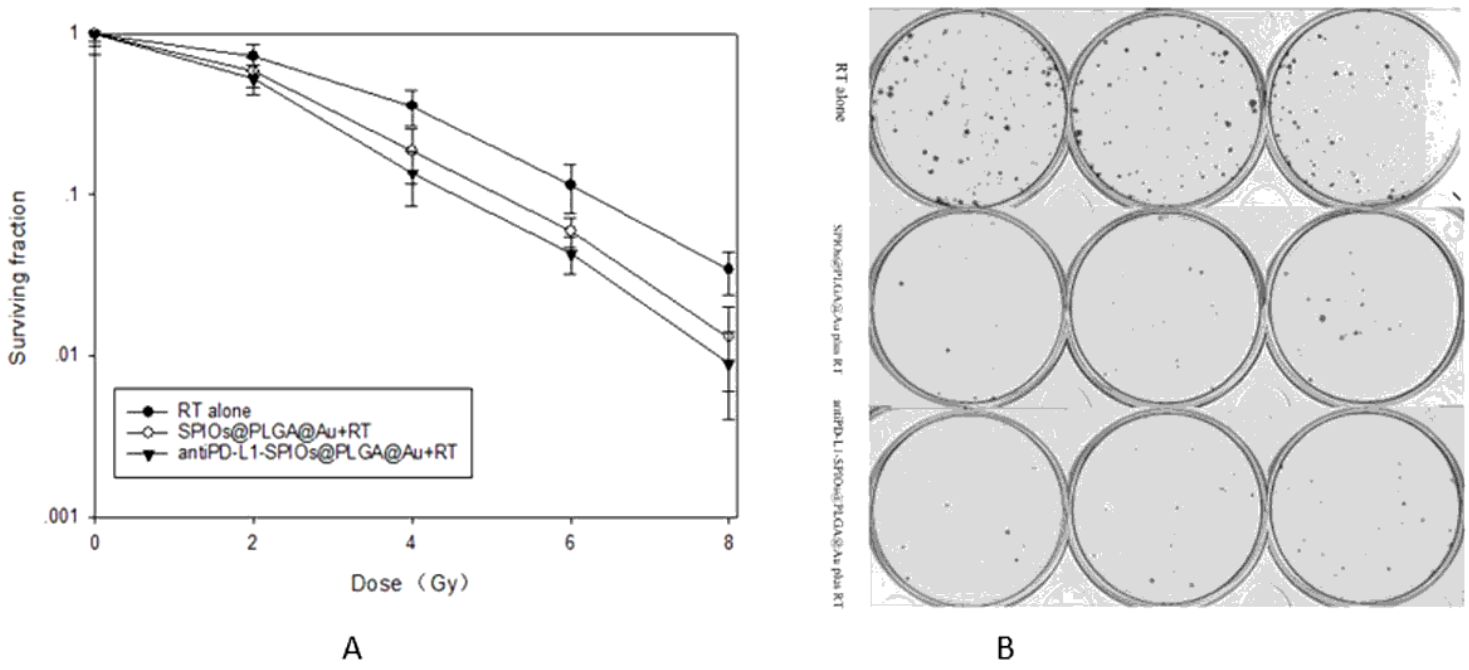

Figure 7

(A) Clonogenic assay of B16F10 cells treated with antiPD-L1-SPIOs@PLGA@Au, SPIOs@PLGA@Au or no nanoparticles and given radiation doses. (B) Clone formation of B16F10 cells irradiated with 4Gy in various groups.

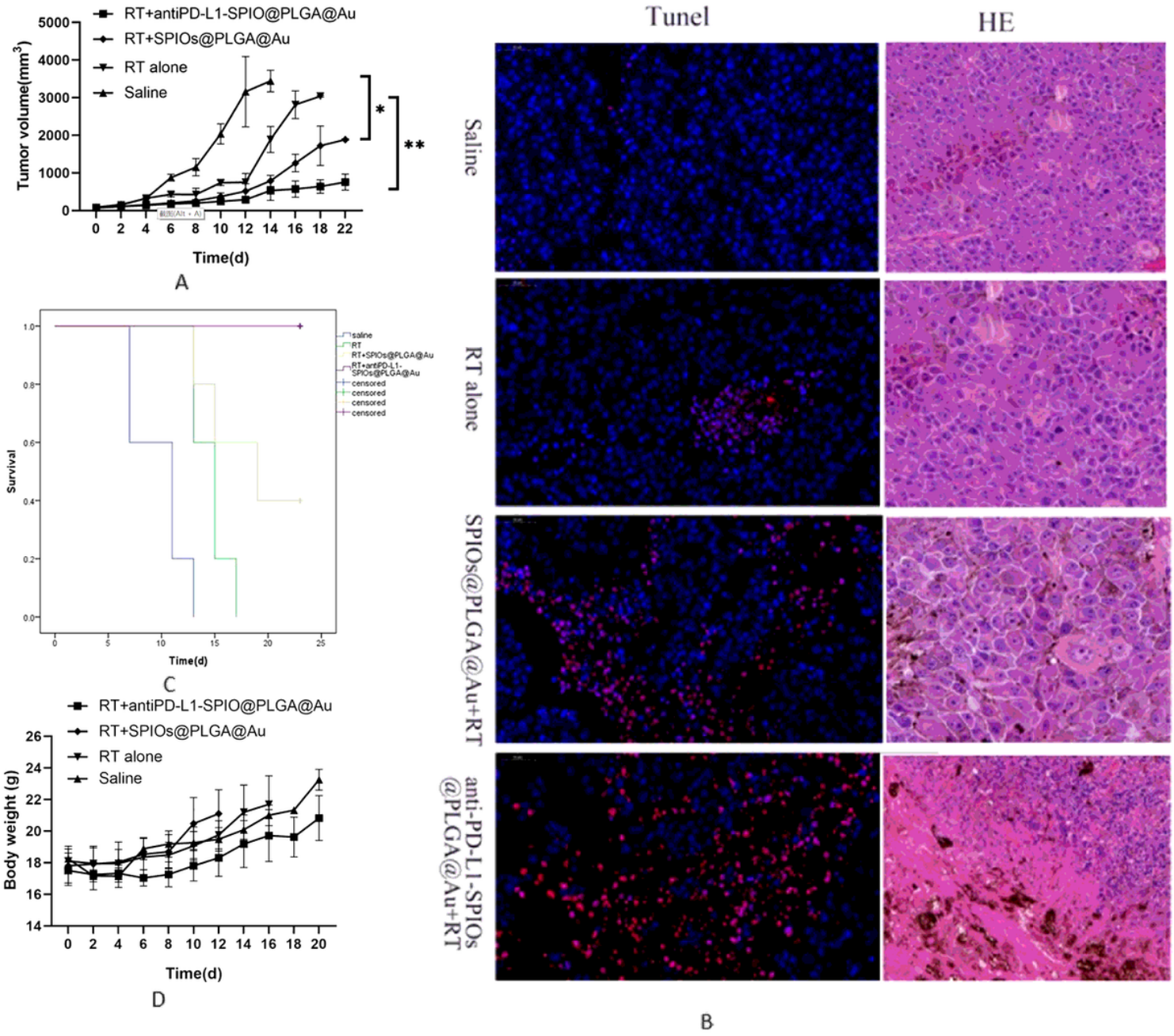

Figure 8

(A) Tumor growth in different treatment groups (n = 4 per group) (B) Tunel and HE staining of tumor tissues after different treatments. (C) Survival curve of tumor-bearing mice in different treatment groups. (D) Body weight changes of B16F10 tumor-bearing mice in different treatment groups. (*p < 0.05, **p < 0.001).

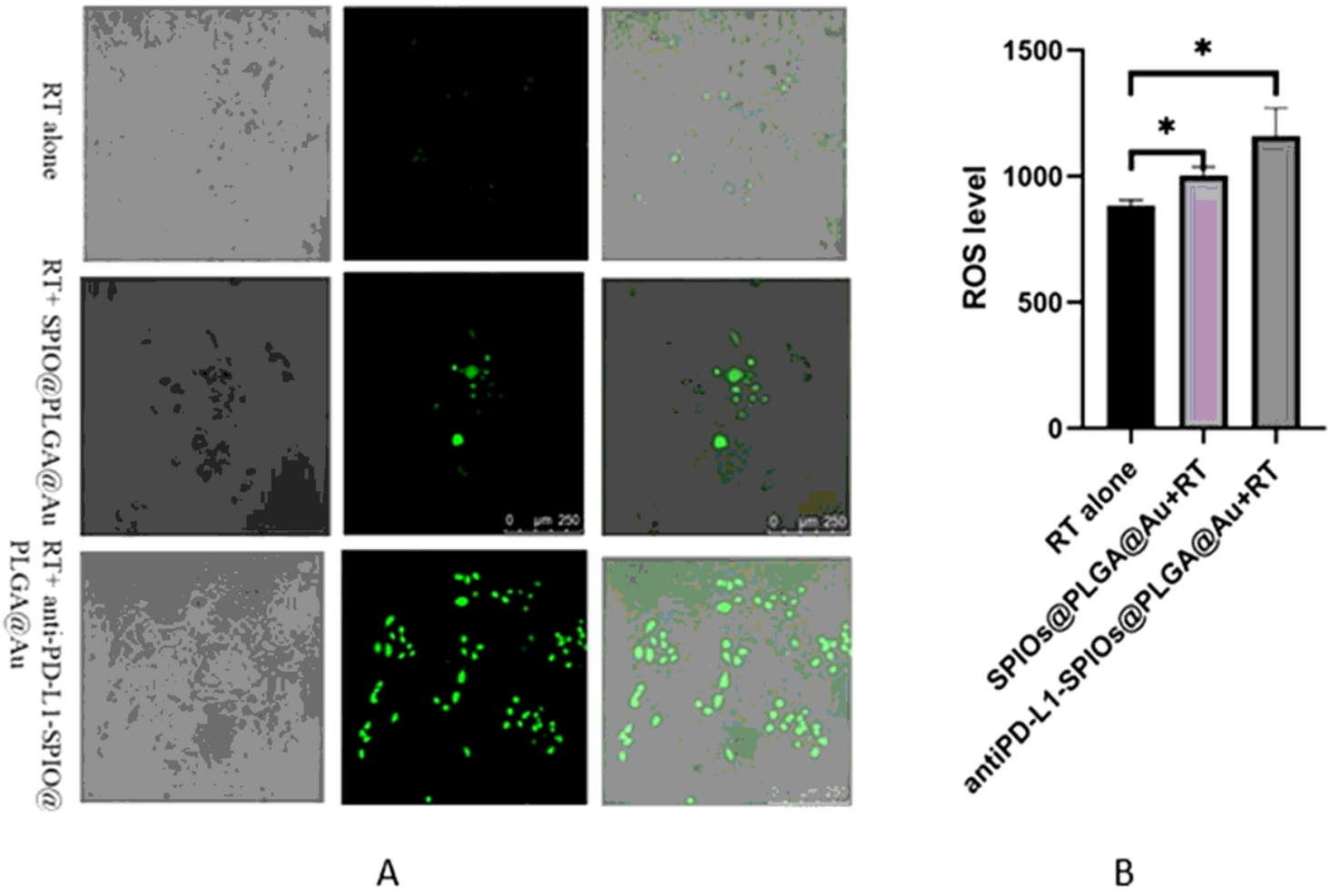

Figure 9

(A) Immunofluorescent imaging of ROS production induced by radiation in B16F10 cells incubated with antiPD-L1-SPIOs@PLGA@Au, SPIOs@PLGA@Au or without nanoparticles. (B) Quantitative analysis of ROS in each treatment group (*<0.05).

Figure 10

Focal fluorescence and quantitative analysis of γ-H2AX B16F10 in different treatment groups (*: P <0.05).

(A) Immunofluorescence image of tumor sections stained with macrophage marker of F4/80 (red), the M2 macrophage marker of CD206 (red) and the M1 macrophage marker of CD86 (green). (B) FCM detects the macrophage phenotype in tumors of different groups (n = 5). (*p < 0.05, **p < 0.001)

Figure 11

(A) Flow cytometry of CD86 (M1 type) and CD206(M2) expression on macrophages after co-culture with different culture components (**: P <0.001).

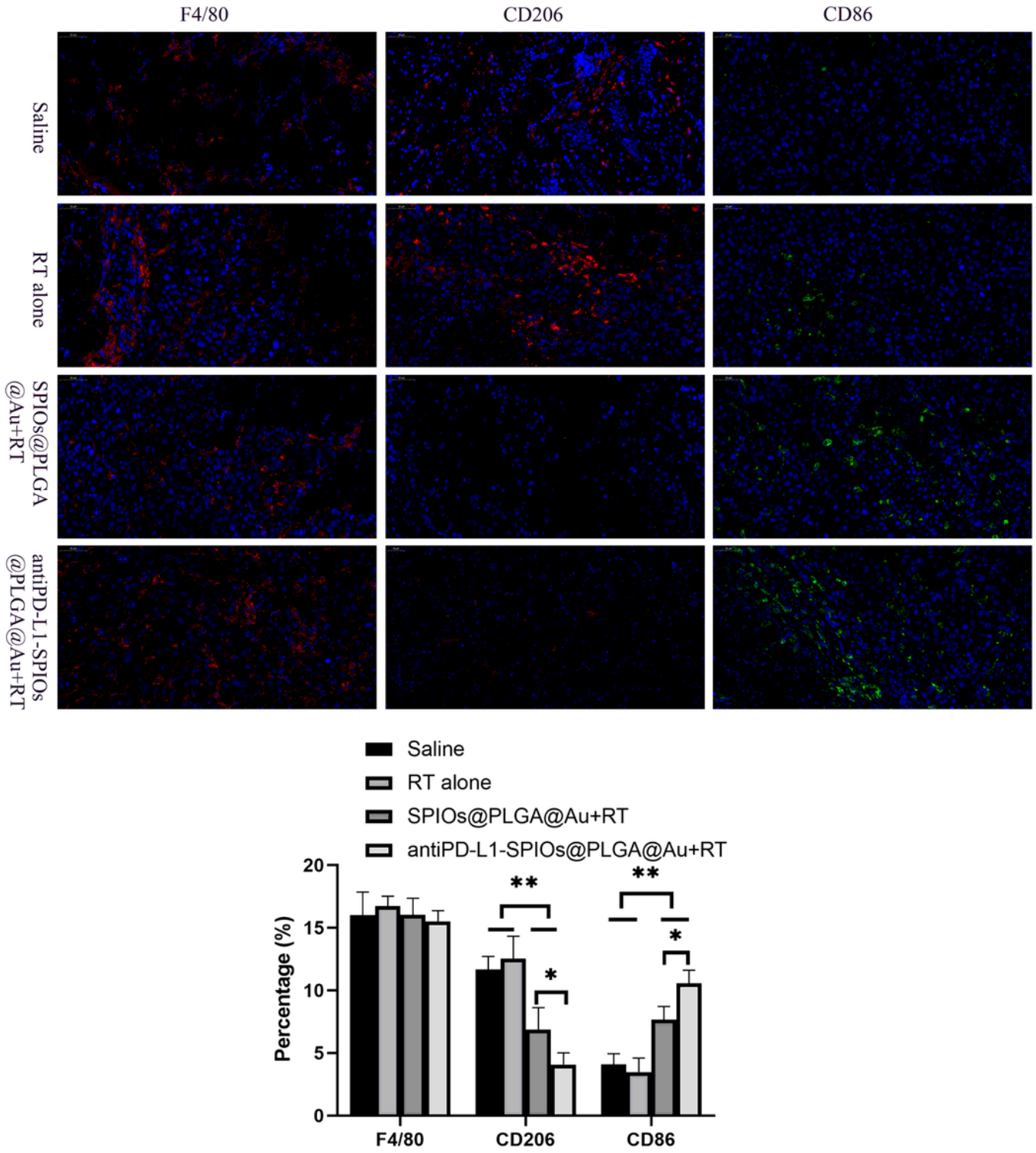

Figure 12

(A) Immunofluorescence image of tumor sections stained with a macrophage marker of F4/80 (red), the M2 macrophage marker of CD206 (red) and the M1 macrophage marker of CD86 (green).

Figure 13

(A) CRT immunofluorescence staining image of tumor tissue; (B) Quantitative analysis of positive area ratio of CRT immunofluorescence staining images of tumor tissues;(C) Western blot results of CRT in different treatment groups; (D) Quantitative analysis of CRT protein western blot results in different treatment groups.

Figure 14

(A) Representative immunofluorescence images of tumor slices stained by anti-CD4 antibody (red). (B) Representative immunofluorescence images of tumor slices stained by anti-CD8 antibody (red). (C) Proportions of tumor-infiltrating CD8+ T cells and CD4+ T cells among in the tumor.

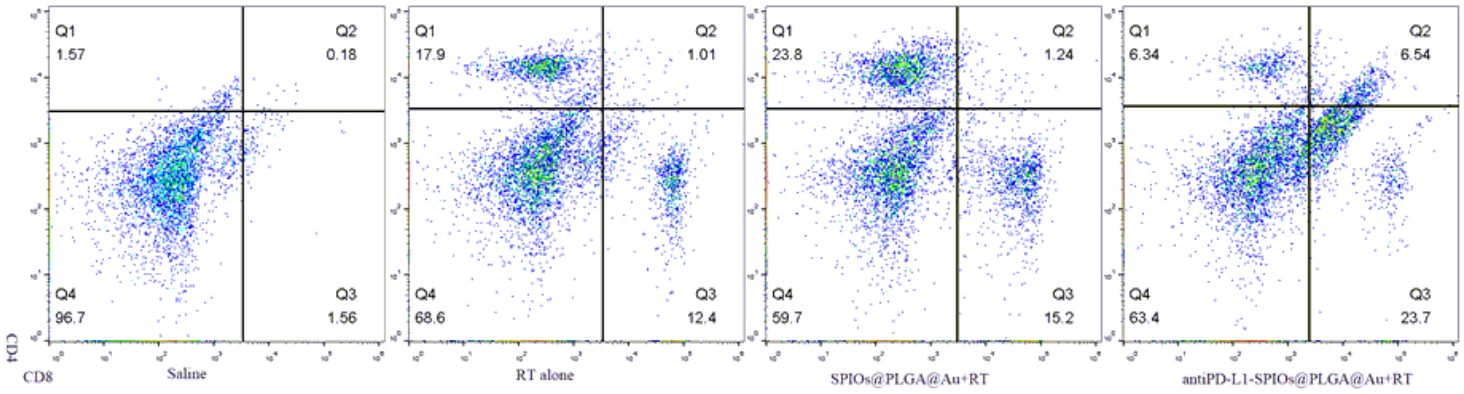

A

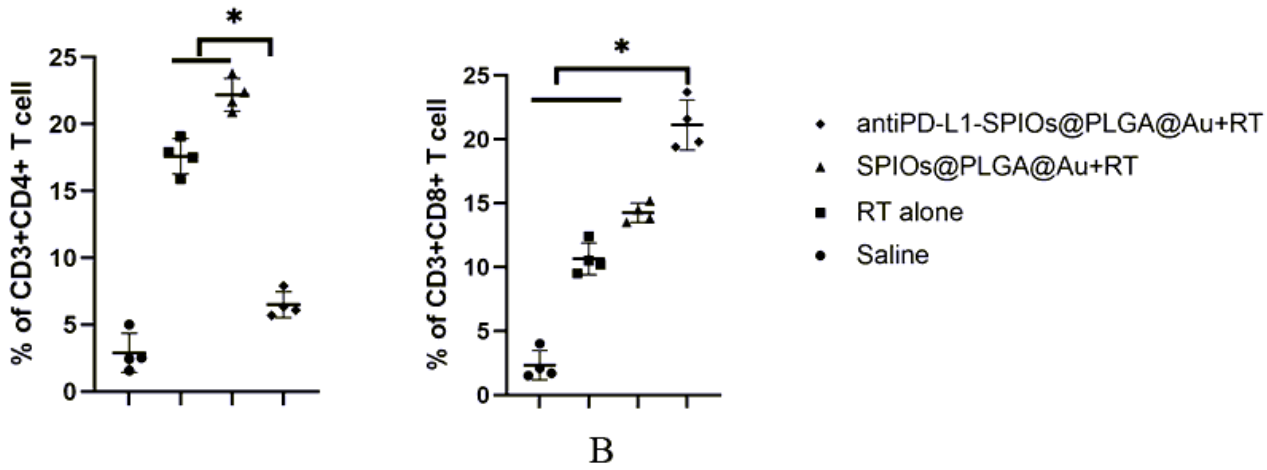

B

Figure 15

(A) Representative flow cytometry plots showing different types of T cells in tumor draining lymph nodes from different groups of mice. (B) Proportions of tumor-infiltrating CD8+ T cells and CD4+ T cells in lymph node.

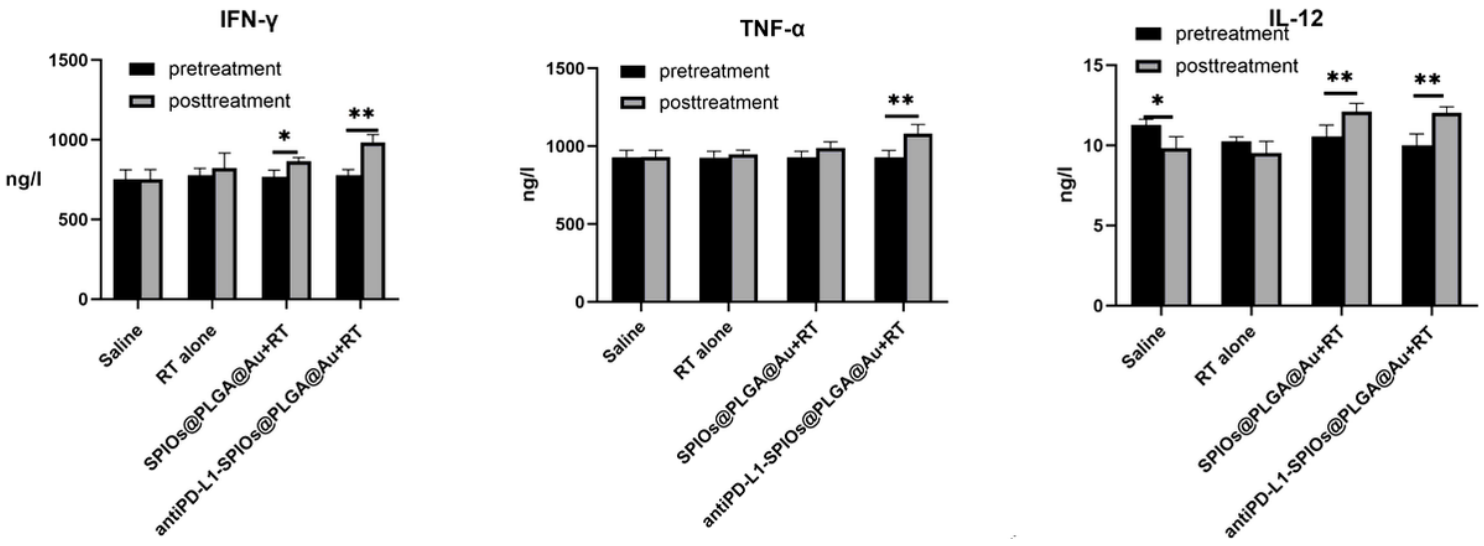

Figure 16

Cytokine levels in sera isolated at day 7 days after various treatment.

Supplementary Files

This is a list of supplementary files associated with this preprint. Click to download.

- FigureS1.tif